Photoelectron recoil in CO in the x-ray region up to 7 keV

E. Kukk,[1] T.D. Thomas,[2] K. Ueda,[3] D. Céolin,[4] S. Granroth,[1] K. Kooser,[1] O. Travnikova,[5,4] D. Iablonsky,[3] P. Decleva,[6] D. Ayuso,[7] R. Püttner,[8] H. Levola,[1] G. Goldsztejn,[5] T. Marchenko,[5,4] M.N. Piancastelli,[5,9] and M. Simon[5,4]

[1] *Department of Physics and Astronomy, University of Turku, FI-20014 Turku, Finland*

[2] *Department of Chemistry, Oregon State University, Corvallis, Oregon 97331, USA*

[3] *Institute of Multidisciplinary Research for Advanced Materials, Tohoku University, Sendai 980-8577, Japan*

[4] *Synchrotron SOLEIL, L'Orme des Merisiers, Saint-Aubin, BP 48, FR-91192 Gif-sur-Yvette Cedex, France*

[5] *Sorbonne Universités, UPMC Univ Paris 6, CNRS, UMR 7614, Laboratoire de Chimie Physique-Matière et Rayonnement, F-75005 Paris, France*

[6] *Dipartimento di Scienze Chimiche, Università di Trieste, and CNR-IOM, 34127 Trieste, Italy*

[7] *Max Born Institute for Nonlinear Optics and Short Pulse Spectroscopy, Max-Born-Strasse 2A, 12489 Berlin, Germany*

[8] *Fachbereich Physik, Freie Universität Berlin, Arnimallee 14, D-14195 Berlin-Dahlem, Germany*

[9] *Department of Physics and Astronomy, Uppsala University, SE-75120 Uppsala, Sweden*

(Dated: March 16, 2018)

ABSTRACT

Carbon 1*s* photoelectron spectra of CO molecules in gas phase were recorded in the tender x-ray energy range, from 2.3 to 6.9 keV. The intensity ratios of individual peaks from ν=0 to 3 within the vibrational progression of the C 1*s* photoelectron spectrum were determined at the various photon energies and are shown to be strongly affected by the photoelectron recoil effect. The experimental vibrational intensity ratios are compared with theoretical predictions at different levels of accuracy. New developments of the recoil model, using generalized Franck-Condon factors, rovibrational coupling, Morse potential energy curves, and accurate angular averaging are presented and applied to the analysis of the experimental results.

I. INTRODUCTION

The carbon monoxide molecule has been the source for many new observations and physical insights obtained by core-level x-ray ionization or excitation. As a common diatomic molecule, its neutral ground state has been characterized with high precision, and its core-ionized states have been investigated by numerous experimental and theoretical works. The carbon 1s photoelectron spectrum of CO is characterized by a clearly defined single vibrational progression with levels up to ν=3 easily visible and it is thus well suited for studying the interplay of the electronic transitions and changes in the molecular geometry. In our recent paper [1], the intensity ratios of the peaks ($v = 1/v = 0$) in the C 1s photoelectron spectrum were obtained over an extended photoelectron kinetic energy range from the C 1s ionization threshold up to 1200 eV. In the simplest approximation, once beyond the resonance effects very close to the threshold, the vibrational peak ratios in the photoelectron spectra (referred to as the *v-ratios* from here on) are expected to be independent of the electron kinetic energy. They are expected to be determined by the Franck-Condon factors, which reflect the changes in molecular geometry upon core ionization; in this particular case the vibrational progression arises from the contraction of the C-O bond. The excitation arising from this source is referred to as "Franck-Condon" excitation.

A more careful inspection of the dependence of the v-ratios on the photoelectron kinetic energy reveals pronounced oscillations hundreds of eV above the ionization threshold and, at even higher energies where these oscillations dampen, the v-ratios continue to increase steadily. We have demonstrated by theoretical modeling [1] that the oscillatory behaviour of the v-ratios, observed also in several other molecules [2–4], is caused by photoelectron scattering on neighboring atoms. The outgoing electron wave from the emitter atom is scattered by the molecular potential; the scattered wave then interferes with the original one and, depending on the wavelength of the electron waves, this interference leads to periodic suppression or enhancement of the wave amplitude. The oscillations in the v-ratio are a manifestation of that interference pattern, persisting even after averaging over all electron emission directions, but the higher order interference terms at shorter wavelengths (higher kinetic energy) quickly dampen.

Another effect, superimposed on these oscillations, is a continuous increase of the v-ratio of the intensity of the ν=1 peak over ν=0, R_{10}. This increase is caused by the photoelectron

recoil effect, where some of the available energy is transferred into internal motion – vibrations and rotations – of the molecule [5–8]. Upon photoionization, an electron is ejected with a certain momentum, and the molecular ion is left with a corresponding equal and opposite momentum, referred to as the "recoil" momentum. Core-level electrons such as C $1s$, which do not participate in molecular bond formation, can be viewed as essentially atomic, bound to a single atomic nucleus. Crucially then, the recoil momentum is initially attached to that particular nucleus, as well as to the center of mass of the entire molecule. Simple total momentum conservation then dictates how this momentum is shared between the translational recoil of the entire molecule and the excitations of the internal degrees of freedom. Since increasing the photoelectron energy also increases the recoil momentum, the momentum and energy transferred to the internal motion also increases. Quantum mechanically, this is seen as an increase in the excitation probabilities of higher vibrational levels, in addition to the Franck-Condon excitations that are always present when the molecular potential changes, independently of the photoelectron energy.

The energy range over which the v-ratios of gas-phase molecules can be investigated is limited by experimental factors – decreasing photoionization cross-sections, low transmission of electron analyzers at high energies, difficulties in obtaining sufficient energy resolution and, most importantly, lack of suitable x-ray sources for gas-phase electron spectroscopy. The earlier investigations of photoelectron recoil effects were carried out at soft x-ray synchrotron radiation beamlines dedicated to gas-phase experiments. The grating monochromators used at these sources limit the practical photon energy range to 1500 eV or less. The present study was carried out at the GALAXIES beamline of the SOLEIL synchrotron which, by combining a crystal monochromator with a gas-phase experimental arrangement and with a dedicated high-energy electron analyzer, dramatically extends the practicable energy range to about 10 keV – covering the so-called tender x-ray region. An advantage of the broader energy range is that it provides an opportunity to obtain reliable data on the $v = 0 \rightarrow 2$ and $v = 0 \rightarrow 3$ transitions, which have not been previously available. Whereas the intensity for the $v = 0 \rightarrow 1$ transition varies approximately linearly with the photoelectron energy, the photoelectron energy dependence of the $v = 0 \rightarrow 2$ and $v = 0 \rightarrow 3$ intensities is described by quadratic and cubic polynomials, respectively, and this behavior becomes apparent only at higher energies than have heretofore been available.

In the tender x-ray region, the steadily increasing recoil effects are transformed from slight modifications to the Franck-Condon-determined vibrational profiles into a major factor determining the v-ratios. Consequently, more stringent tests of our current assumptions are possible and more precise models need to be implemented. Here we discuss a model to deal with these theoretical questions and then compare the theoretical predictions with our experimental results. Finally we consider some further details and implications of the theoretical model.

II. THE RECOIL MODEL

A. Recoil energy and excitations

To see how the photoelectron recoil affects the molecular excitation we consider the ejection of a photoelectron with kinetic energy E_{kin} and linear momentum $\vec{p}_e$ from atom A of a diatomic molecule AB. Momentum conservation requires that the whole molecule undergo a momentum change $\Delta\vec{p}_M = -\vec{p}_e$, which leads to a change in the translational motion of its center of mass. This results in an increase in the average translational energy of the molecule of $\Delta E_{trans} = p_e^2/(2M)$, where M is the molecular mass. On the other hand, the recoil energy of the emitter atom, $\Delta E_A = p_e^2/(2M_A)$, is larger than ΔE_{trans}. The energy difference between these, which we refer to as E_{rec}, goes into internal excitation of the molecule and is given in eq. 1.

$$\begin{aligned} E_{rec} &= \Delta E_A - \Delta E_{trans} \\ &= \frac{p_e^2}{2M}\frac{M_B}{M_A} = E_{kin}\frac{mM_B}{MM_A} \end{aligned} \tag{1}$$

where m is the electron mass. For a diatomic molecule this internal excitation divides between vibrational and rotational excitation according to the projection of $\vec{p}_e$ on the molecular axis. Thus

$$E_{vib} = E_{rec}\cos^2\theta \tag{2}$$

$$E_{rot} = E_{rec}\sin^2\theta \tag{3}$$

where θ is the angle between $\vec{p}_e$ and the molecular axis.

We see from eqs. 1, 2, and 3 that the internal excitation increases linearly with the photoelectron kinetic energy. For a typical photoelectron spectrum the vibrational structure is resolved but the rotational structure is not. To measure the recoil-induced rotational excitation it is necessary to measure the shift of peak centroids relative to an internal standard, as has been done for the valence photoelectron spec-

trum of N_2 [9, 10]. For vibrational excitation it is possible to measure this effect by recognizing that the recoil-induced vibrational excitation (eq. 2) must be reflected in the excitation probabilities of the vibrational energy levels – that is, in the Franck-Condon factors. From an experimental point of view these probabilities are conveniently represented by intensity ratios, $R_{v0} = I_{v'}/I_{v'=0}$, where $I_{v'}$ is the observed intensity for the indicated peak in the spectrum.

These ratios are affected by Franck-Condon excitation, by recoil-induced vibrational excitation, and by the effects of the recoil-induced rotational excitation on the final-state vibrational wavefunctions. In addition, the experimental intensities are determined in systems where the molecules are randomly oriented with respect to the photoelectron direction.

An appropriate theoretical model must take all of these effects into account and we discuss such a model in the following section. However, even without a detailed model certain qualitative conclusions can be drawn and we discuss these in the following paragraphs.

Take CO as an example and assume for simplification that it has zero angular momentum and that we can ignore the one unit of angular momentum associated with dipole ionization. Since the equilibrium bond length shrinks upon ionization, there will be some Franck-Condon profile of vibrational states excited even at low energy excitation. At higher energies we must take into account the recoil-induced ionization. For emission at 0° to the molecular axis, there will be an increase in the vibrational energy, but no change in the energies of the individual vibrational states. Therefore, the increase in vibrational energy must appear as a modification of the Franck-Condon profile, which becomes shifted to a higher average value of the vibrational quantum number, v'. For emission at 90° there will be excitation of rotational motion, leading to a final-state angular momentum of J' given by $J'(J'+1)\hbar^2 = (pR)^2$, where p is the recoil momentum in the center-of-mass system and R is the equilibrium bond length. Within the rigid-rotor approximation, the final-state vibrational wavefunction is independent of J', with the result that the Franck-Condon factors are the same in this case as they are for the case of no recoil-induced excitation. However, the rovibrational energies are shifted to higher values by the rotational energy $J'(J'+1)\hbar^2/(2\mu R'^2)$, where R' is the equilibrium bond length for the ionized molecule and μ is the reduced mass of the molecule.

Thus, we see that the rovibrational profile is dependent on the angle of emission of the photoelectron with respect to the molecular axis. For 0° the rovibrational energies are approximately

equal to $\hbar\omega'(v'+1/2)$, where ω' is the vibrational frequency, and the Franck-Condon profile is shifted to higher values of v'. At 90° the rovibrational energies are approximately equal to $\hbar\omega'(v'+1/2)+J'(J'+1)\hbar^2/(2\mu R'^2)$, but the Franck-Condon factors are approximately the same as the no-recoil values. So far, there has been no observation of these angularly resolved profiles; the only measurements are for angle-averaged profiles. In interpreting these experiments, it is necessary, therefore, to calculate these angle-averaged profiles and to do this we need predictions of the profiles over the angular range from 0° to 90°.

In closer detail, the picture outlined above is not quite correct. The portion of the recoil energy that goes into internal excitation, E_{rec}, is equal to $p^2/(2\mu)$. For emission at 90° the angular momentum is, as noted above, given by $J'(J'+1)\hbar^2 = (pR)^2 = 2\mu E_{rec}R^2$. The rotational energy of the ionized molecule is

$$J'(J'+1)\hbar^2/(2\mu R'^2) = E_{rec}R^2/R'^2 \qquad (4)$$

For carbon 1s ionization of CO $R' < R$, with the result that the rotational excitation is higher than the recoil energy. This extra energy arises from Coriolis coupling. As the newly formed rotating molecule shrinks from the equilibrium bond length of the neutral molecule to the equilibrium bond length of the ionized molecule, the Coriolis interaction leads to a transfer of energy from the vibrational mode to the rotational mode. Thus, the average rotational energy is larger than the recoil energy by $E_{rec}(1/R'^2 - 1/R^2)$ and the average vibrational energy is smaller than the energy expected from the usual Franck-Condon factors by the same amount. The existence of this effect of the Coriolis coupling has previously been explored from a classical point of view [11]. In order to see this effect from a quantum mechanical point of view, it is necessary to explore the effects of the angular momentum on the eigenvalues and eigenfunctions of the rotating oscillator as well as on the Franck-Condon factors that connect the rotating ionized molecule to the initial neutral molecule.

III. THEORETICAL MODELS

A. Generalized Franck-Condon factors

If we are not concerned with recoil-induced excitation of vibrational motion, then the relative intensities, $I_{v'}$, of the rovibrational peaks are given by the usual Franck-Condon factors, FCF:

$$I_{v'} \propto FCF = \left| \int \psi'_{v'J'}(r)\psi_{v=0J}(r)dr \right|^2 \qquad (5)$$

where r is the coordinate along the bond direction. The unprimed symbols refer to the initial state, assumed to be in its vibrational ground state, and the primed symbols refer to the ionized state.

The wavefunctions, ψ_{vJ}, are the r-dependent vibrational wavefunctions for the molecule or ion [12]. If the effects of rotation are included, they are also J dependent and are eigenfunctions of the Hamiltonian

$$\hat{H} = \hat{H}_0 + \frac{J(J+1)\hbar^2}{2\mu r^2} \tag{6}$$

where $\hat{H}_0$ is the Hamiltonian for the oscillator in the absence of angular momentum.

In order to include the effects of recoil-induced excitation it is necessary to use generalized Franck-Condon factors [13, 14]:

$$I_{v'} \propto GFCF(v', J', v, J, p, \theta) = \left| \int \psi'_{v'J'}(r) e^{irp\cos\theta/\hbar} \psi_{v=0J}(r) dr \right|^2 \tag{7}$$

Here p is the magnitude of the recoil momentum (in the center-of-mass system), and θ is the angle of emission of the photoelectron with respect to the molecular axis.

For comparison between experimental observations and predictions it is necessary to average eq. 7 over the initial values of J and the emission angles θ, and to sum it over the final values of J'. For the case at hand, this procedure is more complicated than is necessary. Firstly, in a typical core-electron photoelectron spectrum, the rotational states are not resolved. Secondly, for high-energy photoelectrons J' is likely to be much larger than J. Accordingly, it is appropriate to introduce the simplifying approximations that the initial angular momentum is zero and that the one unit of angular momentum associated with the dipole ionization can be ignored. Then the term in J disappears from the initial-state Hamiltonian and we can replace $J'(J'+1)\hbar^2$ with $(pR)^2 \sin^2\theta$ in the final state Hamiltonian [15]. We can rewrite eq. 7 as

$$GFCF(v', J' = pR\sin\theta, v = 0, J = 0) \left| \int \psi'_{v'pR\sin\theta}(r) e^{irp\cos\theta/\hbar} \psi_{00}(r) dr \right|^2 \tag{8}$$

The left-hand wavefunctions are eigenfunctions of the Hamiltonian

$$\hat{H} = \hat{H}_0 + \frac{(pR)^2 \sin^2\theta}{2\mu r^2} \tag{9}$$

The right-hand wavefunction is the ground-state wavefunction for the neutral molecule.

Evaluation of the generalized Franck-Condon factors, eq. 8, requires that we specify a model and its Hamiltonian. Two possibilities are considered in the following two sections: the linear-coupling model with a rigid rotor, and a Morse potential plus an angular momentum term.

B. The linear-coupling rigid-rotor model

Before looking at the generalized Franck-Condon factors in detail, we consider first a simple model that illustrates the main features of the results that will be seen in the more exact calculations. This is the linear-coupling model, which assumes that the initial- and final-state wavefunctions are harmonic oscillator functions and that the characteristic frequency for the oscillators, ω, is the same for both initial and final states. In addition, for this approximation, we also assume the rigid-rotor approximation, with the result that the effects of the rotational motion on the wavefunctions are ignored. These approximations lead to a semiquantitative picture of what to expect from the more general results.

For the linear-coupling model, the generalized Franck-Condon factors for the transition from the ground vibrational state of the neutral molecule to vibrational state v' of the ion are given by a Poisson distribution [14].

$$P_{v'} = S^{v'} e^{-S}/v'! \tag{10}$$

S includes a contribution from Franck-Condon excitation, S_{FC}, arising from the change in equilibrium bond length between the initial and final states, and a recoil contribution, S_{rec}, arising from the recoil-induced excitation of vibrational motion. S_{FC} can be calculated from the change in bond length, and $S_{rec} = E_{rec}\cos^2\theta/(\hbar\omega)$. The $\cos\theta$ dependence arises because only the component of the recoil momentum along the molecular axis contributes to the vibrational excitation, as indicated in eq. 2. The two terms are additive [14], and we have

$$S = S_{FC} + E_{rec}\cos^2\theta/(\hbar\omega) \tag{11}$$

We see immediately the result discussed qualitatively above that the generalized Franck-Condon distribution broadens (S increases) as $\cos\theta$ increases and more of the recoil momentum contributes to motion along the molecular axis.

For $\theta > 0$ there will be rotational as well as vibrational excitation, and, as a consequence, the rovibrational energies will be given by the expression

$$\begin{aligned} E(v', J') &= (v' + 1/2)\hbar\omega + \frac{J'(J'+1)\hbar^2}{2\mu R^2} \\ &= (v' + 1/2)\hbar\omega + E_{rec}\sin^2\theta \end{aligned} \tag{12}$$

The factor of $\sin^2\theta$ arises because only the component of recoil momentum perpendicular to the molecular axis gives rise to rotational excitation, as indicated in eq. 3. The difference between R and R' is ignored for this example, which is intended to be illustrative rather than quantitative. This approximation is consistent

with the rigid-rotor model. The average value of the excitation energy is given by

$$\langle E(v', J')\rangle = \sum_{v'} E(v', J') \frac{S^{v'} e^{-S}}{v'!} \quad (13)$$

$$= S_{FC}\hbar\omega + E_{rec} + \hbar\omega/2 \quad (14)$$

Eq. 14 is obtained by substituting eqs. 11 and 12 into eq. 13. Thus the average energy (centroid of the rovibrational distribution) is independent of the angle of emission and is equal to the zero-point energy plus the Franck-Condon excitation and the recoil excitation.

By a similar exercise we can show that the variance of the rovibrational distribution is given by the following expression.

$$\left\langle E(v', J')^2 \right\rangle - \langle E(v', J')\rangle^2 = (\hbar\omega)^2 S$$

$$= (\hbar\omega)^2 S_{FC} + \hbar\omega E_{rec}\cos^2\theta \quad (15)$$

Thus the centroid of the rovibrational distribution is independent of θ, but the variance of the distribution varies linearly with $\cos^2\theta$. These features will be seen in the more detailed results discussed below.

From an experimental point of view, it is relatively easy to make a precise measurement of the centroid of an isolated peak, or even the centroids of overlapping peaks of comparable intensity. However measuring the centroid for the entire rovibrational profile is difficult because of the low intensity of the peaks for higher values of v'. These may be too small to provide reliable information, but because of their high v' values they make significant contributions to the centroid. This problem is even more acute for determining the variance. An alternative approach has been to measure the intensity ratios $R_{v0} = I_{v'}/I_0$, which can be used as measures of the recoil-induced excitation, and this is the quantity reported in our experimental results.

For a Poisson distribution we have the following relationships.

$$R_{v'0} = \left(S_{FC} + E_{rec}\cos^2\theta/(\hbar\omega)\right)^{v'}/v'! \quad (16)$$

$$R_{10} = S_{FC} + E_{rec}\cos^2\theta/(\hbar\omega) \quad (17)$$

$$R_{20} = S_{FC}^2/2 + S_{FC}E_{rec}\cos^2\theta/(\hbar\omega) + \left(E_{rec}\cos^2\theta/(\hbar\omega)\right)^2/2 \quad (18)$$

and thus we can expect R_{10} to vary linearly with $\cos^2\theta$ with a slope equal to $E_{rec}/(\hbar\omega)$ and an intercept equal to S_{FC}. For R_{20} we have a quadratic relationship, eq. 18. The first term in this expression arises from direct excitation of the $v' = 2$ state via normal Franck-Condon excitation. The second term represents the process where one unit of the change in v' comes from Franck-Condon excitation and one unit from recoil-induced excitation. The third shows the contribution of two units of excitation by recoil. For the case of CO, the Franck-Condon excitation is strong, with the result that the energy

dependence of R_{20} is dominated by the linear term for small values of E_{rec}. We will see these features in the more detailed calculations presented below.

The discussion above is appropriate for a particular value of θ, that is for a system where the orientation of the molecule with respect to the photoelectron is known. However, for the measurements that have been made so far on recoil effects have involved randomly oriented molecules, and it is, therefore, necessary to find appropriate angular averages. A convenient, but approximate, approach is to average R_{v0} over angles, assuming an isotropic distribution of the photoelectrons in the molecular frame. For R_{10} this gives

$$\langle R_{10} \rangle = S_{FC} + \frac{E_{rec}}{3\hbar\omega} \tag{19}$$

This expression, which since Ref. [7] has been used to predict recoil-induced vibrational excitation, indicates that the observed value of R_{10} should vary linearly with the recoil energy and with the photoelectron energy.

However, the measured quantity, $\langle R_{10m} \rangle$, is not $\langle R_{10} \rangle$ but $\langle I_{v'} \rangle / \langle I_0 \rangle = \langle GFCF_{v'} \rangle / \langle GFCF_0 \rangle$. For the linear-coupling model we show in the appendix, eq. A.9, that

$$\langle R_{10m} \rangle = S_{FC} + \frac{E_{rec}}{3\hbar\omega} - \frac{4}{5}\left(\frac{E_{rec}}{3\hbar\omega}\right)^2 \cdots \tag{20}$$

For low values of the recoil energy $\langle R_{10m} \rangle$ follows the linear dependence of eq. 19, but at higher values of E_{exc} there is a downward quadratic trend. We will see precisely this behavior in the results of the more accurate calculations described below.

The previous discussion has ignored the effects of the rotational motion on the generalized Franck-Condon factors and on the intensity ratios. The ion is initially created with angular momentum J' in a vertical transition at the equilibrium bond length, R, of the neutral molecule. The rotational energy is $J'(J'+1)\hbar^2/(2\mu R^2)$. As the molecule contracts towards the equilibrium bond length of the ion, R', the angular momentum remains constant but the average rotational energy increases to $J'(J'+1)\hbar^2/(2\mu R'^2)$. The additional energy comes from the vibrational energy via Coriolis coupling, with the consequence that the average vibrational energy is lowered by the amount $J'(J'+1)\hbar^2\left(R^2/R'^2 - 1\right)/(2\mu R^2)$. This change must be reflected in the generalized Franck-Condon factors.

We can use the approach that the generalized Franck-Condon factors are given approximately by a Poisson distribution to gain some insight into this question. As described in the

appendix, eq. A.8,

$$\langle R_{10m} J\rangle = S_{FC} + (1-2f)\,\frac{E_{rec}}{3\hbar\omega} - \frac{4}{5}\left((1+f)\,\frac{E_{rec}}{3\hbar\omega}\right)^2 \cdots \quad (21)$$

where $\langle R_{10m} J\rangle$ is the predicted value of the observed ratio including the effects of rotation, and $f = R^2/R'^2 - 1 = 0.093$ for CO. Thus the coefficient of the linear term in eq. 20 is expected to be decreased by the Coriolis effect by about 19%, and the coefficient of the quadratic term is expected to be increased by about the same amount. We will see that this is indeed the case for the more accurate calculations.

The linear-coupling model thus provides a framework within which to understand the results of the more accurate calculations.

C. Morse model

For a more detailed study the linear-coupling rigid-rotor model is replaced by a Morse model. The Morse potential is completely characterized by the frequencies ω_e and ωx_e, and the radius parameter, r_e. For neutral CO, $\omega_e = 2169.81358$ cm^{-1}, $\omega x_e = 13.28831$ cm^{-1}, and $r_e = 1.128323$ Å [16]. For illustrative examples of the theoretical results we have used the following values for carbon 1s ionized CO: $\omega'_e = 2456.765$ cm^{-1}, $\omega x'_e = 10.001$ cm^{-1}, and $r'_e = 1.079005$ Å [1].

It is necessary to average eq. 7 over the initial values of J and over the angle θ and to sum over the values of J'. For the case at hand, however, we can introduce a simplifying approximation. At room temperature, the initial values of J are small, whereas at the photoelectron energies considered here J' is large. Accordingly, we use the approximations that $J = 0$ and that the one unit of angular momentum associated with the photon can be ignored. In this case, we can set $J' \approx pR\sin\theta/\hbar$, or, more accurately, $J'(J'+1) = p^2R^2\sin^2\theta/\hbar^2$, where R is the equilibrium bond length in the neutral molecule.

The wavefunctions $\psi'_{v'J'}(r)$ and $\psi_{v=0J}(r)$ in eq. 7 are eigenfunctions of the Hamiltonian $\hat{H}$ (eq. 6), where $\hat{H}_0$ is the Hamiltonian for the oscillator in the absence of angular momentum. For the present analysis $\hat{H}_0$ is based on the Morse potential. The eigenfunctions and eigenvalues for this Hamiltonian must be evaluated numerically. For this we have used the Numerov method, using a procedure created by Mueller and Huber [17] for Maple. For the ground state, the only eigenfunction needed is for $v = 0$ and $J = 0$. For the ionized state it is necessary to consider a range of v' values and a value of J' appropriate to the recoil energy and angle being considered according to the relationship $J'(J'+1) = (pR)^2\sin^2\theta/\hbar^2$.

Once suitable wavefunctions have been calculated it is straightforward to evaluate the generalized Franck-Condon factors using eq. 8. For the ionized state we also consider a rigid-rotor Hamiltonian

$$\hat{H} = \hat{H}_0 + \frac{J(J+1)\hbar^2}{2\mu R'^2} \tag{22}$$

where R' is the equilibrium bond length for the ion. In this case, the wave functions do not depend on J', and are simply Morse functions, and the eigenvalues are the Morse values plus $J(J+1)\hbar^2/(2\mu R'^2)$.

The eigenvalues are nearly the same for both rigid and nonrigid rotor, differing primarily in the contribution from vibration-rotation interaction, which is present for the nonrigid rotor and absent for the rigid rotor. For the current example this is quite small. When the rovibrational wavefunctions are used in calculating the GFCFs, the vibrational excitation probabilities and the v-ratios are decreased in comparison to the calculation with purely vibrational wavefunctions of a rigid rotor. The vibrational ratios are lower for the nonrigid rotor because of Coriolis coupling between the rotational and vibrational modes. The role of the Coriolis interaction is discussed in more detail below and in ref. [18].

A comparison of the calculated ratios with the observed ones is presented in the following section. A more detailed view of theoretical results is presented in a subsequent section.

IV. EXPERIMENTAL PROCEDURES AND RESULTS

A. Experimental procedures

The results were obtained at the SOLEIL Synchrotron, France, on the GALAXIES beamline equipped with an end station dedicated to hard and tender X-ray photoelectron spectroscopy [19, 20]. Linearly polarized light is provided by a U20 undulator and monochromatized by a Si(111) double crystal monochromator. At some energies it was necessary to reduce the photon flux at the sample in order to avoid nonlinearity effects associated with the readout of the CCD detector of the Scienta spectrometer. This was achieved by introducing Al foil filters of 6 and 12 μm thickness into the beam. The CO sample and the calibration gas argon were introduced into a differentially pumped gas cell.

The photoelectron spectra were recorded by a large acceptance angle EW4000 Scienta hemispherical analyser, optimized for high kinetic energy measurements. The spectrometer was mounted with the lens axis colinear with the polarization vector of the x-rays. In this exper-

iment, the spectrometer was operated at 100-eV pass energy and with the entrance slit of 0.3 mm, except for the photon energy of 6900 eV, at which the larger slit of 0.5 mm was used.

B. Data analysis

The primary goal of the analysis of the photoelectron spectra was to extract accurate values for the v-ratios. In the earlier experiments using the soft x-ray excitation, the combined total energy resolution was sufficient to resolve the vibrational progression in the C 1s spectra, which has the ν=0-1 peak spacing of 302 meV – see Fig. 1a. This figure shows, for reference, a C 1s photoelectron spectra recorded at $h\nu$=400 eV at the PLEIADES beamline of the SOLEIL synchrotron, previously analyzed and reported in Ref. [1]. The Lorentzian lifetime broadening of 92 meV and the vibrational spacings for ν=0-3 were obtained from the least-squares curve fitting of this spectrum; these values were then used in analyzing the new spectra at the tender x-ray region.

In the tender x-ray range various contributions to the practically obtainable resolution combine to make the progression unresolved – see Fig. 1b and 1c. The v-ratios can still be extracted using least-squares curve fitting, but only with careful application of constraints in order to reduce the number of free parameters and to increase reliability.

At each photon energy (spectra for $h\nu$=2500 eV, 2700 eV and 3000 eV are not shown in Fig. 1), a calibration spectrum of Ar 2p photoelectrons was measured with the same settings as for CO. The Ar 2p spin-orbit doublet was fitted with Voigt profiles using the SPANCF macros for Igor Pro [6, 21]. It became apparent that in the photon energy range from 2300 to 3000 eV a single profile could not give a satisfactory representation of the spectral peaks, due to the fact that the photon band from the double-crystal monochromator strongly deviates from the Gaussian shape. However, a statistically near-perfect fit was obtained by using two Voigt profiles of equal Gaussian and Lorentzian widths for each peak. The intensity ratio and energy separation of these two profiles then gave a template for the instrument function, to be applied to the analysis of the CO 1s spectra. The individual peaks in Fig. 1b are in fact composites of two Voigt profiles, obtained as described above. The Ar 2p photolines recorded at $h\nu$=6900 eV, on the other hand, are well described by single Voigt profiles. Here, the monochromator is operated at the 3rd order of diffraction and the optical conditions produce a Gaussian-like photon band. Thus the corresponding CO 1s

spectra in Fig. 1c were also fitted with a single Voigt profile per peak.

Neither the Lorentzian nor Gaussian widths of the Voigt profiles can be directly transferred from the Ar 2p results. The former differs due to different core-hole lifetimes. In the curve fitting, the fixed value of 92 meV from the reference spectrum at $h\nu$=400 eV was used. The latter has contributions, in addition to the purely instrumental ones from the monochromator and electron analyzer, also from both the translational and rotational Doppler broadenings, which are sample-specific. The instrumental contribution can be derived from the Ar 2p spectra after removing the translational Doppler broadening for argon. These various contributions are summarized in Table 1. As can be seen, the convolution of the three contributions (total) accounts fairly well for the experimental (fitted) Gaussian component of the peak width.

Table I. Spectral line widths in C 1s photoelectron spectra, as Gaussian FWHM (in meV). Dplr_t and Dplr_r refer to the translational and rotational Doppler broadenings, respectively.

$h\nu$(eV)	Instr.	Dplr_t	Dplr_r	Total	Fitted
2300	195	106	99	243	253
2500	200	111	104	251	261
2700	231	116	109	280	290
3000	252	123	115	303	310
6900	210	192	180	337	344

C. Vibrational intensity ratios

The intensity ratios were calculated from the intensities for the first four peaks in the vibrational progression. These intensities were obtained from the spectra by least-squares curve fitting as described above. In addition to the peak intensities, the energy of the ν=0 peak, the common Gaussian width and the background intensity were the adjustable parameters in the fit. The v-ratios R_{10}, R_{20} and R_{30} are shown in Fig. 2 together with their values in the soft x-ray range from earlier measurements (for R_{10} and R_{20}) [1]. The error bars represent the statistical uncertainty in the peak intensity values; an additional systematic component to the error can arise from uncertainties in the peak separation values or in the Lorentzian lifetime width.

The figure also shows theoretical predictions at various levels of accuracy. The lower-accuracy models are included for two reasons: they have been used in the analysis of the recoil effects in earlier publications [1], they are also easier to apply and computationally much less demanding.

First, the dashed lines in Fig. 2 represent the v-ratios obtained using the linear-coupling model as presented in Section III B, with the ground-state fundamental frequency of 269.0 meV and the bond contraction of $\Delta R =$

−5.0 pm. This calculation also neglects the effects of molecular rotation. The averaging over the electron emission angles in the molecular frame, however, was done accurately, according to Eq. 20 (and similar expressions for the higher v-ratios). The accurate angular averaging is the cause of the visible deviation downwards from the expected linear form of R_{10} and has a similar effect on the other curves. The curves have a significant vertical offset with respect to the experimental values for both R_{10} and R_{30}, although they happen to match very well with the experiment in the case of R_{20}. These offsets are due to the neglect of both the anharmonicity and the change of the frequency. On the other hand, the slope of the curves is in a good agreement with the data points, which suggests that the linear-coupling model, although crude, is still useful as an easy-to-apply first estimate of the recoil-induced vibrational excitations even in the tender x-ray range.

The next step towards a more accurate model is given by the dash-dotted black line in Fig. 2 (labeled "harmonic"), which represents the v-ratios obtained using the generalized Franck-Condon factors (GFCFs) as described in Section III A. The model now accounts for the fundamental frequency change from 269.0 to 301.9 meV upon core ionization but retains the harmonic oscillator approximation. The calculation also still does not include the effects from molecular rotations. Although the simple formulae of the LCM model are not applicable any more, analytical forms of the harmonic wavefunctions can be used in GFCFs. The result is a clear improvement for R_{10}, but is much worse for R_{20} and R_{30} in terms of vertical offsets. However, the recoil-related behavior (the slopes) does not change from the linear-coupling model. This is expected, since it is the ground-state fundamental frequency, not that of the ionic state, that affects the strength of the recoil excitations [14].

Next, wavefunctions obtained numerically from Morse potential energy curves were used in calculating the GFCFs and v-ratios (thin red lines in Fig. 2), giving a good agreement with the experiment both in offsets and slopes (except for the high-energy point in R_{30}). For the ground state the parameters of the Morse potential are $r_e = 1.128323$ Å, $\hbar\omega_e = 0.269022$ eV, and $\hbar\omega x_e = 0.00164754$ eV [16]. These are the same values that we have used to obtain the results described in the theoretical section.

For the ionized state we have derived new values for $\hbar\omega'_e$ (0.3057 ± 0.0004 eV) and $\hbar\omega x'_e$ (0.00189 ± 0.00015 eV) from analyzing 10 low-energy, high-resolution spectra for C 1s ionization of CO, taken at various times and various synchrotron facilities (ALS, MAX II, SPring-8,

and SOLEIL). The value for r'_e can be determined from reported values of the bond-length change, ΔR, which are close to -5.0 pm. However, almost all of these values are based on analysis of vibrational spectra for core-ionized CO in the low-energy region, where the intensities are strongly affected by scattering and interference. Consequently we have chosen to use the value of -4.96 pm, which has been obtained in a multireference average coupled-pair functional calculation [22], and is independent of these effects.

Accurate angular averaging was performed numerically, first calculating the GFCFs for a range of emission angles relative to the molecular axis for each emission energy and then averaging with the weighting factors that correspond to an isotropic distribution.

Finally, we add the effects of molecular rotations, as discussed in Section III. This is the computationally most expensive model, requiring numerical integration of the rovibrational wavefunctions of the core-ionized state for every emission energy and angle. For the ground state, according to the approximations described in Section III, we need only the single wavefunction ψ_{00}. The thick red curves representing this model show the expected behavior – that the slopes of the v-ratios are lowered due to the Coriolis coupling between the vibrational and rotational motions. This effect is as large as 20% (see Sections III B and V C) and is an essential element of the recoil model.

This model, which includes rotational effects, gives poorer agreement with the experiment for R_{10} than do the less complete models. The data are not sufficient at this point to assess the significance of this discrepancy, which could arise from larger uncertainties in the data than we have indicated, from unknown systematic experimental errors, or from effects that may have been omitted from the theoretical analysis (such as possible anisotropy for the photoelectron emission).

Figure 2a reproduces (by the red dotted line labeled "DFT") also earlier scattering calculations [1] that were extended up to a photoelectron kinetic energy of 8 keV, in order to demonstrate that the v-ratios in the tender x-ray region are essentially free from the intramolecular scattering induced oscillations. The theoretical treatment of Section III (which neglects scattering) is therefore well suited for this energy range. The scattering calculation matches closely with the GFCF recoil model using Morse potentials, but neglecting rotational coupling.

V. THEORETICAL RESULTS

Here we consider some more detailed results of the theoretical models that have been discussed earlier.

A. Rovibrational profiles

As a specific illustration, we have done a set of calculations with the momentum in the center-of-mass system, p, equal to 8 au. This corresponds to a photoelectron energy of 2667 eV. The average energy of excitation due to the change in equilibrium bond length upon ionization (Franck-Condon excitation) is 2609.39 cm^{-1} and the recoil excitation is 561.86 cm^{-1} for a total excitation of 3171.25 cm^{-1}. If the emission is perpendicular to the axis, $J' \approx 17$. The calculations have been done for five angles corresponding to $\cos\theta = 0(0.25)1$. Results from these calculations are seen in Fig. 3.

Fig. 3a shows the rovibrational profiles for two angles of emission with respect to the molecular axis, 0° (black) and 90° (grey). In each case the generalized Franck-Condon factors for each value of v' are plotted against the rovibrational energy for that v'. We see here the behavior expected from the earlier discussion. For $\theta = 0°$ the Franck-Condon distribution is broadened, but the rovibrational energies are those for a molecule with no rotational excitation. By contrast, for $\theta = 90°$ the Franck-Condon factors are very close to those expected for no recoil-induced excitation (shown as the crosses), but the rovibrational energies are shifted to higher values by the rotational energy. In spite of the obvious visible differences in the two profiles, the average rovibrational energies (centroids) are the same, 3170.20 cm^{-1} at 0° and 3171.23 cm^{-1} at 90°, as we expect from the discussion of the linear-coupling model [23].

Also shown in Fig. 3a are lines representing the bars dispersed with Gaussian function with a width of 2400 cm^{-1} (300 meV), which is typical of the resolution that can be obtained at this photoelectron energy. The features that are seen in the stick spectra are still evident in these dispersed spectra.

Although the centroids are independent of angle, this is not the case for the variances, which are plotted against $\cos^2\theta$ in Fig. 3b. The straight line in this figure is a linear fit to the calculated points, and we see that the fit is quite good, in keeping with our expectations from eq. 15.

Fig. 3c shows the intensity ratios R_{10} (solid circles) and R_{20} (open circles), plotted against $\cos^2\theta$. The solid line shows a linear fit to the R_{10}, which fits well, in keeping with the linear-coupling model. For R_{20} a quadratic fit (dashed

line) is necessary, in keeping with eq. 18. The quadratic term, which goes as E_{rec}^2 is, however, relatively small compared with the linear term.

B. The Coriolis effect

Forty eigenvalues have been calculated in this exercise, covering the range in v' from 0 to 7 and in J' from 0 to 17. We expect these energies to be described by the relationship

$$E(v', J')/hc = (v' + 1/2)\omega'_e - (v' + 1/2)^2\omega x'_e + B'J'(J' + 1) - \alpha'(v' + 1/2)J'(J' + 1) \quad (23)$$

Fitting the calculated eigenvalues to this equation gives the spectroscopic constants for the ionized molecule, which are summarized in Table II. Also shown here are the original values of ω'_e and $\omega x'_e$ that were used to generate the Morse potential from which the wavefunctions and eigenvalues were derived. We see that there is satisfactory agreement between the input set and the derived set.

Table II. Spectroscopic constants from fitting the eigenvalues. Also shown are the input values of ω_e amd ωx_e. cm^{-1}.

Constant	Fit	Input
ω'_e	2456.74	2456.76
$\omega x'_e$	10.003	10.001
B'	2.119	
α'	0.013	

We can apportion eq. 23 into two equations giving approximately the contributions of vibrational motion, on the one hand, and rotational motion, on the other.

$$E(v')/hc \approx (v' + 1/2)\omega'_e - (v' + 1/2)^2\omega x'_e - \alpha'(v' + 1/2)J'(J' + 1)/2 \quad (24)$$

$$E(J')/hc \approx B'J'(J' + 1) - \alpha'(v' + 1/2)J'(J' + 1)/2 \quad (25)$$

(The rotational-vibrational term, which has been divided equally between the two forms of motion, is quite small.) Using these equations together with the constants in Table II and the generalized Franck-Condon factors for 90° we can obtain values for the average vibrational and rotational excitation at 90°. These are 2556.7 cm^{-1} and 614.7 cm^{-1}. The first of these is to be compared with the Franck-Condon excitation that would be found in the case for $\theta = 0°$ where there is no rotational excitation. This is 2609.4 cm^{-1}, which is greater than the 90° value by 53 cm^{-1}. The second is to be compared with the recoil energy, 561.9 cm^{-1}, which is smaller by 53 cm^{-1}. These differences arise from Coriolis coupling.

The ionized molecule is created in a vertical transition with the bond length of the neutral molecule. At this point the vibrational excitation – 2609.4 cm^{-1} – is equal to the extra

potential energy arising because the ion is not at its equilibrium distance. The rotational energy, equal to $BJ'(J'+1)$, is, at this point, equal to the recoil energy, E_{rec}. As the molecule shrinks towards its equilibrium radius the angular momentum remains constant and the rotational energy increases. This increase in energy is taken from the vibrational energy by the Coriolis interaction. The rotational energy averaged over a vibrational cycle is $B'J'(J'+1)$. Thus the average rotational energy is greater than the recoil energy by the amount

$$\begin{aligned}\Delta E_{rot} &= J'(J'+1)(B'-B) \\ &= \frac{p^2R^2}{2\mu}\left(\frac{1}{R'^2}-\frac{1}{R^2}\right) \\ &= E_{rec}\left\{R^2/R'^2-1\right) \end{aligned} \tag{26}$$

as noted in the introduction. For carbon 1s ionization of CO, the two bond lengths are $R = 1.128323$ Å and $R' = 1.079005$ Å. With these values $R^2/R'^2 - 1 = 0.0935$ cm^{-1} and $\Delta E_{rot} = 53$ cm^{-1}, as observed.

This decrease in the vibrational energy is reflected in the generalized Franck-Condon factors, as can be seen in Fig. 3a. Here the grey bars show the generalized Franck-Condon factors in the case where there is recoil-induced angular momentum; the crosses show the Franck-Condon factors when there is no recoil excitation. For $v' = 0$, the factor for the former is greater than that for the latter. For $v' = 1$, they are nearly the same and for $v' > 1$ the the factors for no recoil are greater. Thus, in this case ($R' < R$) the recoil-induced rotational excitation leads to a shift in the Franck-Condon distribution and to the observed lowering of the average vibrational energy.

C. Averaging over angles

The foregoing discussion has dealt with photoelectron spectra measured at specific angles with respect to the molecular axis. However, up to the present, no angular resolved measurements of recoil-induced excitation have been made. Reported results have involved measurements that are averaged over all angles. In these experiments the most easily measured quantity has been the ratio of the intensity for $v' = 1$ to that for $v' = 0$, the so-called v-ratio, R_{10}. It is, therefore, appropriate to develop predictions for this angle-averaged ratio.

In the case of the linear-coupling model, we see from eq. 17 that R_{10} varies linearly with $\cos^2\theta$. In Fig. 3c we see that the results from the Morse potential follow this prediction fairly closely. Consequently, we can take as one mea-

sure of R_{10} averaged over angles as

$$\begin{aligned}\langle R_{10}\rangle &= S_{FC} + E_{rec}\left\langle \cos^2\theta\right\rangle/\hbar\omega \\ &= S_{FC} + E_{rec}/(3\hbar\omega) \end{aligned} \quad (27)$$

(assuming that the distribution of photoelectrons is isotropic with respect to the molecular axis). Since E_{rec} is proportional to the photoelectron energy, it follows that $\langle R_{10}\rangle$ varies linearly with the photoelectron energy. This is a convenient approximation and has been used in the past to provide predictions of the recoil-induced vibrational excitation. Values of $\langle R_{10}\rangle$ calculated from the Morse results are plotted versus the photoelectron energy as the open squares points in Fig. 4. The dotted line in this figure is a fit of a quadratic function to the points. The fitting parameters are listed in Table III, where we see that the quadratic term is very small; the values are well fit by a linear function, in accordance with the linear-coupling model, eq. 27.

Table III. Parameters of the lines fitting the points in Fig. 4.

	linear	quadratic
$\langle R_{10}\rangle$	3.20×10^{-5}	-4.7×10^{-12}
$\langle R_{10m}\rangle$	3.20×10^{-5}	-7.94×10^{-10}
$\langle R_{10m}J\rangle$	2.61×10^{-5}	-9.37×10^{-10}

Although $\langle R_{10}\rangle$ is easily calculated and provides a convenient guide to estimate the effects of recoil-induced vibrational excitation, it is not the quantity that is measured in an experiment. The photoelectron spectra that are measured give the intensities, $I_{v'}$, for each final vibrational state, averaged over all emission angles. Therefore, the measured values of R_{v0} are given by the expression

$$\langle R_{v0m}\rangle = \langle I_{v'}\rangle / \langle I_0\rangle \quad (28)$$

where the averages on the right-hand side are taken over all angles of emission. This quantity differs from $\langle R_{10}\rangle$, as can be seen in Fig. 4, where $\langle R_{10m}\rangle$ is plotted as the open circles. The dashed line represents a fit of a cubic polynomial to these points; the linear and quadratic coefficients are listed in Table III. From these parameters, we see that the two quantities agree at low photoelectron energies, but that $\langle R_{10m}\rangle$ becomes nonlinear at high energies. We can understand this behavior by considering the linear-coupling model.

In the discussion of the linear-coupling model we have seen that

$$\langle R_{10m}\rangle = S_{FC} + \frac{E_{rec}}{3\hbar\omega} - \frac{4}{5}\left(\frac{E_{rec}}{3\hbar\omega}\right)^2 \cdots \quad (29)$$

The linear term is the same as in eq. 27, in agreement with the linear terms shown in the first two rows of Table III. The quadratic term for $\langle R_{10}\rangle$ is not significant, whereas for $\langle R_{10m}\rangle$ it is and leads to the downward turn of the

dashed curve. From eq. 29 we can see that the quadratic term should be approximately equal to $-4/5$ of the square of the linear term, or, in this case about -8.20×10^{-10}. The actual value for the Morse results, listed in Table III, is -7.94×10^{-10}, in approximate agreement with this expected value.

The results indicated by curves a and b in Fig. 4 do not contain the effects of rotational motion on the generalized Franck-Condon factors. These effects are included in the solid circles, c, designated by the label $\langle R_{10m} J \rangle$. The solid curve is a fit of a quartic function to the points, with the linear and quadratic coefficients listed in Table III. We see that these results differ from those in which the rotational excitation has not been considered. In particular the slope of 2.61×10^{-5} for C is about 19% lower than the value of 3.20×10^{-5} for a and b, indicating that the effects of the rotational excitation are noticeable even at low photoelectron energies. Similarly the quadratic term for c is about 18% higher than that for b. These values are in accord with the predictions of the linear-coupling model discussed earlier

VI. CONCLUSIONS

The present study demonstrates experimentally that in the tender x-ray region the photoelectron recoil effects become a major factor in determining the vibrational structure of the photoemission spectrum. These effects are observed clearly for the first time not only for the single-quantum recoil excitation from the ground vibrational level, but also for higher recoil excitations and combined recoil and Franck-Condon excitations. This much more extensive experimental data has necessitated also further developments in the theoretical models for treating recoil, such as the use of generalized Franck-Condon factors in actual numerical calculations, accurate angular averaging, use of Morse potentials and incorporating rovibrational coupling into the model. In this paper, we have applied and tested these developments in the particular case of C 1s photoemission in CO. We saw that the simplest, pen-and-paper model, the linear-coupling model, is still quite useful even in the tender x-ray region as the first approximation, if one is specifically interested in the recoil contributions to the v-ratios. However, clear overall improvement is obtained by employing GFCFs and accurate Morse potentials for the ground and ionized states. Furthermore, including the rovibrational coupling was shown theoretically to have a significant impact on the v-ratios as it redistributes the recoil energy from the vibrational to rotational degrees of freedom. It has not yet been proven con-

clusively that the inclusion of the rovibrational coupling actually brings the model to a better agreement with the experiment, but we anticipate that further investigations in the tender x-ray region will shed light on this as well as on the questions of whether there are more approximations in the recoil model that need to be revised, such as the isotropic emission assumption.

VII. ACKNOWLEDGEMENTS

Funding from the Academy of Finland and from COST Action No. CM1204 XLIC is acknowledged. The authors greatly appreciate the help from the GALAXIES beamline staff during the experiments.

VIII. APPENDIX

Appendix: Averaging over emission angles. A simple model

A simple model provides insight into the results of averaging over emission angles for both the case in which the rotational excitation is ignored and the case in which it is included. We start with the approximation that the generalized Franck-Condon factors that describe the rovibrational intensity distribution, P_v, are given by a Poisson distribution.

$$P_v = S^v e^{-S}/v! \tag{A.1}$$

We also assume that the rovibrational levels are spaced harmonically with frequency ω. Although neither of these approximations is accurate, the results obtained using these approximations aid in understanding those obtained from the more complete calculations.

For a Poisson distribution, the average energy (relative to the energy of the lowest energy state of the distribution) is equal to $S\hbar\omega$. This energy contains contributions from the Franck-Condon excitation, $S_{FC}\hbar\omega$, the recoil energy, $E_{rec}\cos^2\theta$, and the Coriolis correction, $-E_{rec}\sin^2\theta\left((R/R')^2-1\right)$. Thus

$$\begin{aligned} S\hbar\omega &= S_{FC}\hbar\omega + E_{rec}\cos^2\theta \\ &\quad -E_{rec}\sin^2\theta\left((R/R')^2-1\right) \\ S &= S_{FC} + \frac{E_{rec}}{\hbar\omega}\cos^2\theta - f\frac{E_{rec}}{\hbar\omega}(1-\cos^2\theta) \\ &= \left[S_{FC} - f\frac{E_{rec}}{\hbar\omega}\right] + \left[(1+f)\frac{E_{rec}}{\hbar\omega}\right]\cos^2\theta \\ &= A + B\cos^2\theta \end{aligned} \tag{A.2}$$

where $f = (R/R')^2 - 1$ and the terms A and B replace the bracketed quantities. The angle-

averaged generalized Franck-Condon are then

$$\begin{aligned}\langle GFCF_v\rangle &= \int_0^{\pi/2} \exp\left(-A - B\cos^2\theta\right) \\ &\quad \frac{\left(A + B\cos^2\theta\right)^v}{v!}\sin\theta d\theta \\ &= \frac{e^{-A}}{\sqrt{B}}\int_0^{\sqrt{B}} e^{-x^2}\frac{(A+x^2)^v}{v!}dx \end{aligned} \tag{A.3}$$

where the substitution $x^2 = B\cos^2\theta$ has been made in the last line. Specifically,

$$\langle GFCF_0\rangle = \frac{e^{-A}}{\sqrt{B}}\int_0^{\sqrt{B}} e^{-x^2}dx \tag{A.4}$$

$$\langle GFCF_1\rangle = \frac{e^{-A}}{\sqrt{B}}\int_0^{\sqrt{B}} e^{-x^2}(A+x^2)dx \tag{A.5}$$

The angle-averaged expression for R_{10} is

$$\begin{aligned} R_{10} &= \langle GFCF_1\rangle \,/\, \langle GFCF_0\rangle \\ &= A + \frac{\int_0^{\sqrt{B}} x^2 e^{-x^2}dx}{\int_0^{\sqrt{B}} e^{-x^2}dx} \end{aligned} \tag{A.6}$$

Expanding the two integrands in a Taylor series and integrating gives

$$R_{10} \approx A + \frac{B/3 - B^2/5\cdots}{1 - B/3\cdots} \approx A + \frac{B}{3} - \frac{4}{5}\left(\frac{B}{3}\right)^2\cdots \tag{A.7}$$

Replacing the symbols A and B with their definitions gives

$$\begin{aligned} R_{10} &= S_{FC} - f\frac{E_{rec}}{\hbar\omega} \\ &\quad + (1+f)\frac{E_{rec}}{3\hbar\omega}\left(1 - \frac{4}{15}(1+f)\frac{E_{rec}}{\hbar\omega}\cdots\right) \\ &= S_{FC} + (1-2f)\frac{E_{rec}}{3\hbar\omega} \\ &\quad -\frac{4}{5}\left((1+f)\frac{E_{rec}}{3\hbar\omega}\right)^2\cdots \end{aligned} \tag{A.8}$$

If we ignore the effect of the Coriolis interaction, then $f = 0$ and we have

$$R_{10} = S_{FC} + \frac{E_{rec}}{3\hbar\omega} - \frac{4}{5}\left(\frac{E_{rec}}{3\hbar\omega}\right)^2\cdots \tag{A.9}$$

[1] E. Kukk, D. Ayuso, T. D. Thomas, P. Decleva, M. Patanen, L. Argenti, E. Plésiat, A. Palacios, K. Kooser, O. Travnikova, S. Mondal, M. Kimura, K. Sakai, C. Miron, F. Martín, and K. Ueda. Effects of molecular potential and geometry on atomic core-level photoemission over an extended energy range – the case study of CO molecule. *Phys. Rev. A*, 88:033412, 2013.

[2] E. Plésiat, L. Argenti, E. Kukk, C. Miron, K. Ueda, P. Decleva, and F. Martin. Intramolecular electron diffraction in vibrationally resolved k-shell photoionization of methane. *Phys. Rev. A*, 85:023409, 2012.

[3] K. Ueda, C. Miron, E. Plésiat, L. Argenti, M. Patanen, K. Kooser, D. Ayuso, S. Mondal, M. Kimura, K. Sakai, O. Travnikova, A. Palacios, P. Decleva, E. Kukk, and F. Martín. Intramolecular photoelectron diffraction in the gas phase. *J. Chem. Phys.*, 139:124306, 2013.

[4] D. Ayuso, M. Kimura, K. Kooser, M. Pata-

nen, E. Plsiat, L. Argenti, S. Mondal, O. Travnikova, K. Sakai, A. Palacios, E. Kukk, P. Decleva, K. Ueda, F. Martn, and C. Miron. Vibrationally resolved b 1s photoionization cross section of BF_3. *The Journal of Physical Chemistry A*, 119:5971, 2015.

[5] W. Domcke and L.S. Cederbaum. Electronic recoil effects in high-energy photoelectron spectroscopy. *J. Electr. Spectr. Rel. Phenom.*, 13: 161, 1978.

[6] E. Kukk, K. Ueda, U. Hergenhahn, X.-J. Liu, G. Prümper, H. Yoshida, Y. Tamenori, C. Makochekanwa, T. Tanaka, M. Kitajima, and H. Tanaka. Violation of the Franck-Condon principle due to recoil effects in high energy molecular Core-Level photoionization. *Phys. Rev. Lett.*, 95, 2005.

[7] T. Darrah Thomas, Edwin Kukk, Rami Sankari, Hironobu Fukuzawa, Georg Prümper, Kiyoshi ueda, Ralph Püttner, James Harries, Yusuke Tamenori, Takahiro Tanaka, Masamitsu Hoshino, and Hiroshi Tanaka. Recoil excitation of vibrational structure in the carbon 1s photoelectron spectrum of CF[sub 4]. *J. Chem. Phys.*, 128:144311, 2008.

[8] Edwin Kukk, T.Darrah Thomas, and Kiyoshi ueda. Recoil effects in molecular photoemission. *J. Electr. Spectr. Rel. Phenom.*, 183:53, 2011.

[9] T. D. Thomas, E. Kukk, H. Fukuzawa, K. Ueda, R. Püttner, Y. Tamenori, T. Asahina, N. Kuze, H. Kato, M. Hoshino, H. Tanaka, M. Meyer, J. Plenge, A. Wirsing, E. Serdaroglu, R. Flesch, and E. Rühl. Photoelectron-recoil-induced rotational excitation of the $B^2\Sigma_u$ state in N_2. *Phys. Rev. A*, 79:0225006, 2009.

[10] T. D. Thomas, E. Kukk, T. Ouchi, A. Yamada, H. Fukuzawa, K. Ueda, R. Püttner, I. Higuchi, Y. Tamenori, T. Asahina, N. Kuze, H. Kato, M. Hoshino, H. Tanaka, A. Lindblad, and L. J. Sæthre. Valence photoelectron spectroscopy of N_2 and CO: Recoil-induced rotational excitation, relative intensities, and atomic orbital composition of molecular orbitals. *J. Chem. Phys.*, 133:174312, 2010.

[11] T. D. Thomas. Coriolis interaction and the division of energy between vibrational and rotational excitation induced by photoelectron recoil. *Phys. Rev. A*, 90:052504, 2014. doi: 10.1103/PhysRevA.90.052504.

[12] $\psi(r) = R(r)r$, where $R(r)$ is the radial wavefunction for the diatomic molecule.

[13] F. Gel'mukhanov, P. Salek, and H. Ågren. Vibrationally resolved core-photelectron spectroscopy as an infinite-slit interferometry. *Phys. Rev. A*, 64:012504, 2001.

[14] T. D. Thomas and K. Ueda. Recoil-induced vibrational excitation in inner-shell photoelectron spectra: Beyond the linear coupling model. *J. Electr. Spectr. Rel. Phenom.*, 195: 101, 2014.

[15] What is the appropriate value for R? For a Morse wavefunction it is not r_e. Other choices are $\langle r \rangle$, $\sqrt{\langle r^2 \rangle}$, and $1/\sqrt{\langle 1/r^2 \rangle}$. A strong argument can be made for using the last of these,

and that is what we have done.

[16] NIST Standard Reference Database Number 69. http://webbook.nist.gov/chemistry/, 2016.

[17] M. Mueller and H. Huber. Solution of the schroedinger equation by the numerov-method for any given one-dimensional potential. Technical Report http://www.chemie.unibas.ch/˜huber/ Numerov/Numerov.html, Institut fuer Physikalische Chemie, Universitaet Basel, 2000.

[18] T. D. Thomas. Coriolis interaction and the division of energy between vibrational and rotational excitation induced by photoelectron recoil. *Phys. Rev. A*, 90:052504, 2014.

[19] D Céolin, JM Ablett, D Prieur, T Moreno, J-P Rueff, T Marchenko, L Journel, R Guillemin, B Pilette, T Marin, et al. Hard x-ray photoelectron spectroscopy on the GALAXIES beamline at the SOLEIL synchrotron. *J. Electr. Spectr. Rel. Phenom.*, 190:188–192, 2013.

[20] J-P Rueff, JM Ablett, D Céolin, D Prieur, Th Moreno, V Balédent, B Lassalle-Kaiser, JE Rault, M Simon, and A Shukla. The GALAXIES beamline at the SOLEIL synchrotron: inelastic x-ray scattering and photoelectron spectroscopy in the hard x-ray range. *Journal of synchrotron radiation*, 22(1):175–179, 2015.

[21] E. Kukk, G. Snell, J. Bozek, W.-T. Cheng, and N. Berrah. Vibrational structure and partial rates of resonant auger decay of the n 1s$\rightarrow 2\pi$ core excitations in nitric oxide. *Phys. Rev. A*, 63:062702, 2001.

[22] T. X. Carroll, K. J. Børve, L. J. Sæthre, J. D. Bozek, E. Kukk, J. A. Hahne, and T. D. Thomas. Carbon 1s photoelectron spectroscopy of CF_4 and CO: search for chemical effects on the carbon 1s hole-state lifetime. *J. Chem. Phys.*, 116:10221, 2002.

[23] The small differences between these and between either of these and the expected value of 3175.25 cm^{-1} arise from approximations made in the numerical evaluation of the wavefunctions and eigenvalues.

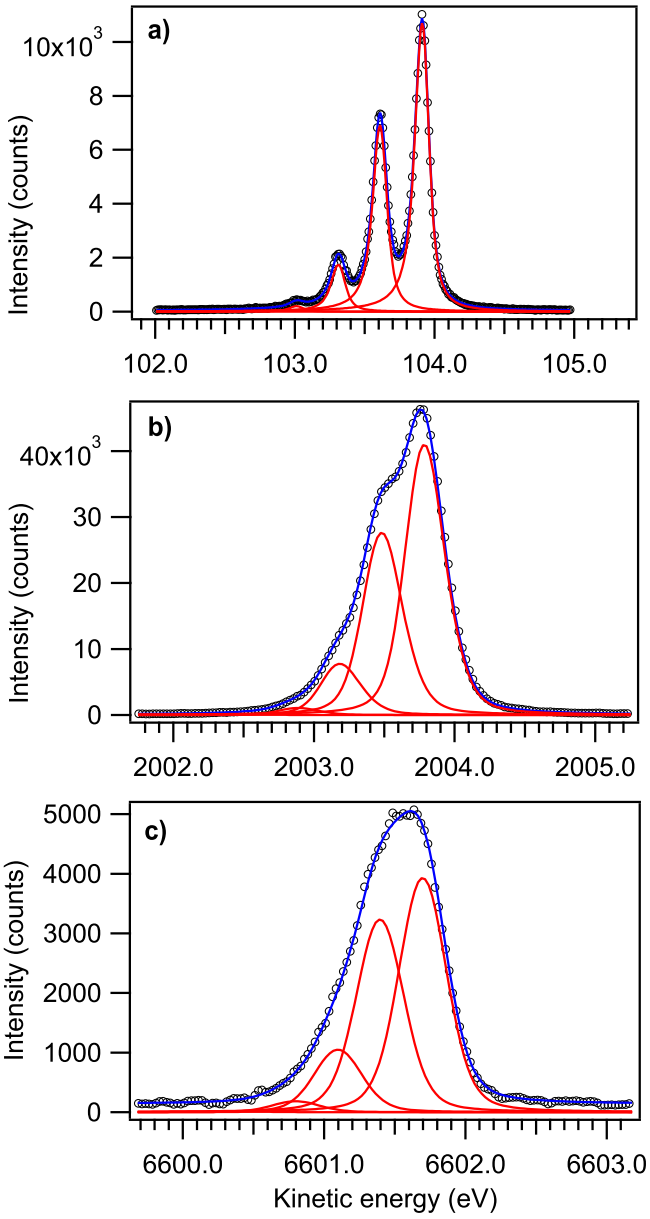

Figure 1. Carbon 1s photoelectron spectra of CO at a) $h\nu$=400 eV, b) $h\nu$=2300 eV and c) $h\nu$=6900 eV. Circles – experiment, red curves – vibrational peaks, blue curve – their sum.

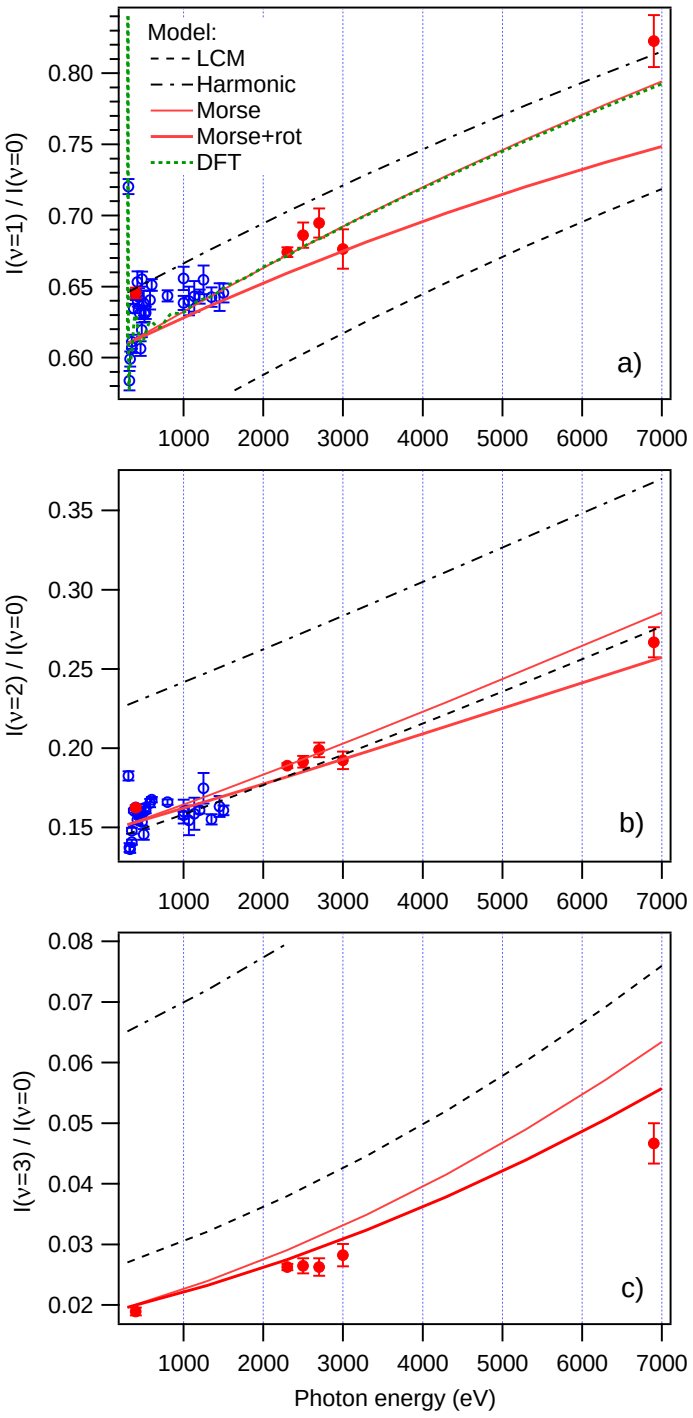

Figure 2. V-ratios in the C 1s photoelectron spectra. Blue circles – earlier measurements [1]; red filled circles – present data and the reference at $h\nu$=400 eV. Dashed black line – LCM; Dash-dotted black line – harmonic oscillator; thin red line – Morse oscillator and thick red line – Morse oscillator with rovibrational coupling. Dotted green line in panel a (mostly overlapping with the "Morse" curve) is static exchange DFT scattering calculations extended from Ref. [1].

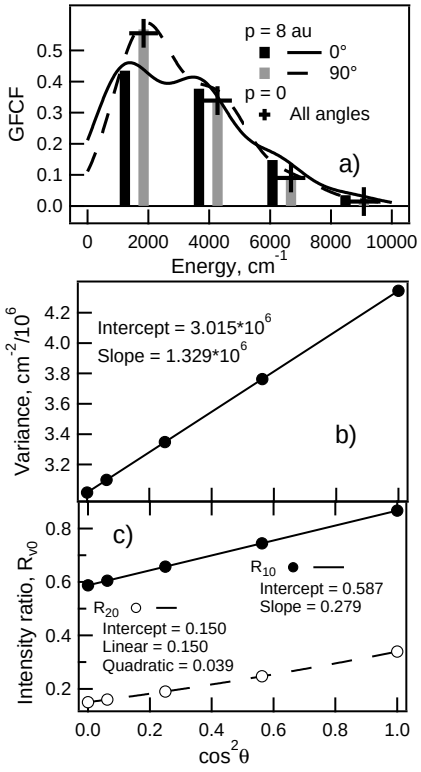

Figure 3. a. Generalized Franck-Condon factors for 0° (black) and 90° (grey) emission of a photoelectron with a center-of mass momentum of $p = 8$ au. Plotted against the rovibrational energy. The lines show the same results dispersed with a Gaussian with a FWHM of 2400 cm^{-1}. The crosses show the Franck-Condon factors for $p = 0$. b. Variances of the rovibrational distribution plotted against $\cos^2\theta$. The line shows a linear fit to the points. c. Intensity ratios R_{v0} for $v' = 1$ (closed circles) and 2 (open circles), plotted against $\cos^2\theta$. The solid line shows a linear fit and the dashed line a quadratic fit.

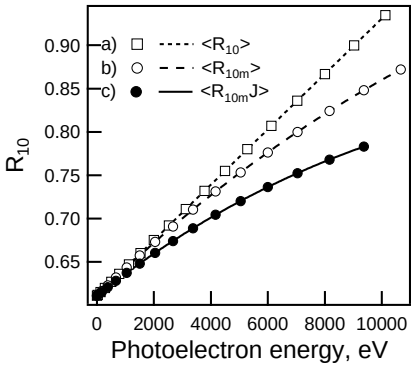

Figure 4. Average values of R_{10} calculated by three different approaches. a: R_{10} averaged over angles. b: $\langle I_1 \rangle / \langle I_0 \rangle$. c: Same as c, except that the rotational potential has been included. The lines show fits of polynomials to the calculated results.